Nanoscale

Accepted Manuscript

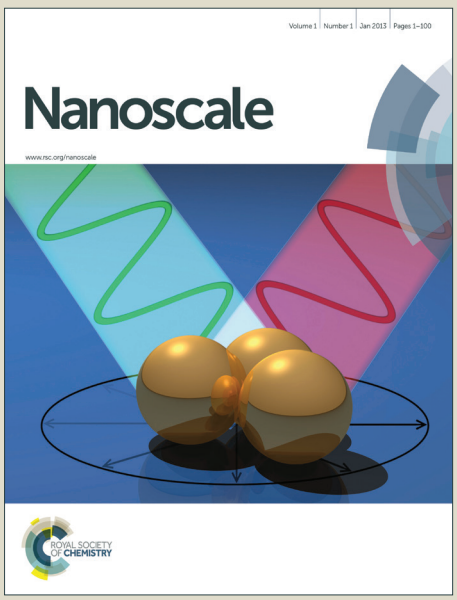

ROYAL SOCIETY OF CHEMISTRY

www.rsc.org/nanoscale

Sub-10nm transparent all-around-gated ambipolar ionic field effect transistor

Seung-Hyun Lee[a,†] , Hyomin Lee[b,c,†], Tianguang Jin[a] , Sungmin Park[b],

Byung Jun Yoon[c], Gun Yong Sung[d], Ki-Bum Kim[a,*] and Sung Jae Kim[b,*]

[a] Department of Materials Science and Engineering, Seoul National University, Korea,

[b] Department of Electrical and Computer Engineering, Seoul National University, Korea,

[c] Department of Chemical Engineering, POSTECH, Korea,

[d]Department of Material Science and Engineering, Hallym University, Korea

[†]Those authors contributed equally

[*]Corresponding Author's E-mail: Ki-Bum Kim (kibum@snu.ac.kr),

Sung Jae Kim (gates@snu.ac.kr)

ABSTRACT

In this paper, we developed a versatile ionic field effect transistor (IFET) which has an ambipolar function for manipulating molecules regardless of their polarity and can be operated at wide range of electrolytic concentrations (10^{-5}M~1M). The IFET has circular nanochannels radially covered by gate electrodes, called "*all-around-gate*", with an aluminum oxide (Al_2O_3) of a near-zero surface charged oxide layer. Experimental and numerical validations were conducted for characterizing the IFET. We found that the versatility is originated from the zero-charge density of oxide layer and all-around-gate structure which increase the efficiency of gate effect 5 times higher than a previously developed planar-gate by capacitance calculations. Our numerical model adapted Poisson-Nernst-Planck-Stokes (PNPS) formulations with additional nonlinear constraints of a fringing field effect and a counter-ion condensation and the experiment and numerical results were well matched. The device can control the transportation of ions at severe concentration up to 1M electrolyte which resembles a backflow of a shale gas extraction process. Furthermore, while traditional IFETs can manipulate either positively or negatively charged species depending on the inherently large surface charge of oxide layer, the presenting device and mechanism provide effective means to control the motion of both negatively and positively charged molecules which is important in biomolecule transport through nanochannels, medical diagnosis system and point-of-care system, etc.

INTRODUCTION

Recent advances in nano-fabrication methods enable to fabricate rigorous and definite nano-sized structure for various scientific and engineering applications. Nanostructure possesses unique scientific and technological properties that microstructure cannot exhibit. Especially, as decreasing the size of nanostructure below 100nm, the structure had a perm-selectivity which let only counter-ions can pass through below a critical electrolyte concentration. The perm-selectivity was reported to be depending on the magnitude and polarity of surface charge density and bulk electrolyte concentration. Thus, the active control of the surface charge density at wide range of electrolyte concentration has been drawn significant attentions in both scientific and engineering field[1-6] for manipulating the motion of charged species and this has become one of the important fields in nanofluidics research. The emerging application fields of nanofluidc system were energy harvesting[1, 2], biosensors[3, 4], backflow from shale gas extraction port[5] or desalinations of seawater[6] which enable to create a huge market that never have existed. Those applications were fundamentally originated from controlling the motion of charged species passing through a nanostructure and, therefore, the cost-effective/on-demand/sensitive control has become the most important practical issue of nanofluidic researches.

Various passive types of modulating the motion of a charged species in nanofluidic system were reported such as changing the viscosity of solution in the nanochannel[7], utilizing mechanical friction between DNA and nanopore[8], coating an adhesive material on nanochannel[9] and surface treatment for changing the surface potential[10, 11]. Those platforms employed passive methods which were unable to change the behavior of charged species on-demand, once the devices were fabricated. In contrast, ionic field effect transistor (IFET) can provide an active method which enables to enhance, diminish or even reverse the behavior of charged species *in situ* by introducing gate potential. However, traditional IFETs can

manipulate either positively or negatively charged species depending on the inherently large surface charge of oxide layer and they demanded either high gate voltage or low electrolyte concentration for changing surface charge density[11-16]. Traditional fabrication method of IFET was principally made by SiO_2[11-13, 15, 16] and nanoporous membrane[14, 17, 18]. While they had easy-fabrication and relatively high uniformity, these materials had high surface charge density which led to a unipolar behavior[11-16]. The reason why the unipolar behavior occurs is that induced surface potential by gate voltage cannot overcome a polarity of inherent surface potential. Due to this characteristic, a traditional IFET can only control the same polarity of charged species with the surface charge of nanochannel. In addition, a planar gate structure in which a gate electrode installed only one wall of nanochannel can modulate the surface charge density at the wall and thus, the efficiency of applying gate voltage would become lower than all-around-gate structure which had a gate electrode at entire surface of nanochannels. Therefore, as previously suggested as "*an ideal structure for field effect reconfigurable nanofluidic diodes would be dual split-gates with a gate-all-around structure and a sub-10 nm nanochannels of a neutral surface*"[16, 19], we have developed a novel design of all-around-gate structure, with 7.5 nm radius nanochannels and minimal surface charge density using Al_2O_3, which has the surface charge density of -1.5 mC/m^2, in this work. Firstly, all-around-gate structure was adapted to increase the efficiency of gate effect at least more than 5 times compared to planar-gate structure. This high efficiency led to obtain an ionic field effect at high electrolyte concentration up to 1 M. Secondly, we deposited Al_2O_3 which have low surface charge density for enabling a polarity independent control. As a result, our device showed an ambipolar behavior at I_D-V_G measurement. The experimental ambipolar effects were validated by numerical simulation with a fringing field effect and a counter-ion condensation which had not been considered as major factors. The experimental and numerical results were in line with our logical procedures and well-matched.

MATERIALS AND METHODS

While the presenting all-around-gated IFET device was fabricated based on a previously reported method[20, 21], advanced features such as transparency was upgraded in this work and its fabrication process was summarized in Figure 1(a). Detailed description can be found in supporting information. We measured the ionic current (I_D) for different gate voltage (V_G) with KCl buffer solution at pH 7 in the concentration range from 10^{-5} M to 1 M. The fluidic chambers were covered with PDMS and Ag/AgCl electrodes were connected on both sides of the chambers. In order to infiltrate water into the thin nanochannel, oxygen plasma was treated for enhancing hydrophilicity[19] and ethanol was filled first and then it was replaced by water for ensuring the wetting. We measured the electric data using the parameter analyzer (Agilent 4156C) in the homemade dark box which blocked the electrical noise. The current was measured as follows. First, drain voltage (V_D) increased from 0V to +2 V at 0.25 V/min for low concentration and 0.5 V/min for high concentration, respectively. After 5 min delay time, V_D decreased from 0 V to -2 V at the same voltage step. For each concentration of KCl, the microchannel was refreshed for 10 minutes with the same solution using a rotary pump. The measurements without the application of gate voltage were repeated until the results were reproduced. For a high concentration case such as 10^{-1} M and 1 M, serious precipitation occurred inside the microchannels. To prevent it, we added refresh step at each change of gate voltage. Leakage current (a current from source to gate) was simultaneously measured for confirming the proper operation.

NUMERICAL SCHEME

Domain definition

The numerical domain to describe the ion transport through the IFET was depicted in Figure 2. To reduce computational cost, we simulated for single channel and then, multiply the number of fabricated nanochannels and each numerical quantity to compare with the experimental results. Cylindrical coordinate was adopted for circular cross-sectional nanochannel. The gate electrode and the oxide layer were omitted in our numerical domain, but they affected on the boundary conditions of the electrokinetic system. Thus the empty space of the gate electrode played as a geometrical constriction. The constriction of the nanochannel positioned near the center of the channel (denoted as A) had 10 um length and 7.5 nm radius. The rest of the nanochannel (denoted as B) had 5 um length and 50 nm radius, respectively, so that the total length of the nanochannel was 20 um. Source and drain reservoirs were connected at left and right side of nanochannel, respectively. Note that the schematic in Figure 2(a) was exaggerated in aspect ratio and the actual domain was shown in Figure 2(b). Although the reservoir dimensions should be larger than the length of the nanochannel for the consideration of the entrance effect inside the reservoirs[22], our 1 um reservoirs were enough to simulate the system regardless of the entrance effect by obtaining similar results with the reservoir size of 1 um, 5 um and 20 um. This was because major variations of electrokinetic quantities were occurred near the gate electrode. Governing equations for describing the gate modulation such as the Poisson-Boltzmann equation and the Laplace equation were independently solved as similar as literatures[23-26], so that the number of degree of freedom could be reduced remarkably. The detailed Poisson-Nernst-Planck-Stokes formulation and proper boundary conditions were shown in supporting information.

General description for metal-oxide-electrolyte (MOE) system

In usual MOE system, the surface charge density is obtained from simple algebraic equations independent from governing equations. In various literatures[23-26], the MOE system was approximated to series capacitors by equivalent electrokinetic circuit models. Using those models, zeta potential and surface charge density modulated by gate voltage can be analyzed by solving simple algebraic equations. However, those equations are only valid in the planar-type MOE system. Therefore, those models should be reformulated to be applicable to the cylindrical MOE system which is our system. When the Stern layer and the chemistry of oxide/electrolyte interface are neglected[25, 27], the charging behavior of the MOE system can be described by the following set of 1D ordinary differential equations based on Gouy-Chapmann theory in case of symmetric electrolyte.

$$\frac{1}{r}\frac{\mathrm{d}}{\mathrm{d}r}\left(r\frac{\mathrm{d}\varphi}{\mathrm{d}r}\right)=\frac{2ZFc_0}{\varepsilon_f}\sinh\left(\frac{ZF\varphi}{RT}\right) \quad \text{at } 0<r<R_f, \tag{1}$$

$$\text{and } \frac{1}{r}\frac{\mathrm{d}}{\mathrm{d}r}\left(r\frac{\mathrm{d}\Phi}{\mathrm{d}r}\right)=0 \quad \text{at } R_f<r<R_f+d_{ox}. \tag{2}$$

In the above, φ is the electric potential in electrolyte, Φ is the electric potential in oxide layer, c_0 is the bulk concentration, F is the Faraday constant, ε_f is the electrical permittivity of the electrolyte, R_f is the radius of the nanofluidic channel, d_{ox} is the oxide layer thickness, and Z is ion valence. Equation (1) is the Poisson-Boltzmann equation expressed as cylindrical form to describe the potential distribution inside nanochannel and equation (2) is the Laplace equation describing the potential distribution within oxide layer. Because we neglect the Stern layer, zeta potential is approximately equal to surface potential, $\zeta=\varphi|_{R_f}$, directly given by gate voltage, V_G. Thus, the modulated zeta potential corresponding to V_G can be obtained by solving equations (1) and (2) with following boundary conditions.

$$\frac{\mathrm{d}\varphi}{\mathrm{d}r}=0 \qquad \text{at } r=0, \tag{3}$$

$$\varphi = \Phi \qquad \text{at } r = R_f \,, \tag{4}$$

$$-\varepsilon_f \frac{\mathrm{d}\varphi}{\mathrm{d}r} + \varepsilon_{ox} \frac{\mathrm{d}\Phi}{\mathrm{d}r} = \sigma_0 \qquad \text{at } r = R_f \,, \tag{5}$$

$$\text{and } \Phi = V_G \qquad \text{at } r = R_f + d_{ox} \,, \tag{6}$$

where ε_{ox} is the electrical permittivity of the oxide layer and σ_0 is the inherent surface charge density on oxide/electrolyte interface which is near-zero value in our ambipolar IFET system, while the typical value of σ_0 is high enough to have unipolar electrical response[12, 13]. Equation (3) is the condition for axis of symmetry, equations (4) and (5) describe oxide/electrolyte interface, and equation (6) is the voltage condition by gate electrode. Equation (5) implies the discontinuity of electric displacement field at interface where Gauss's law for electrostatic field should be satisfied. Since above formulation is valid to a system where the full length of nanochannel is completely covered by a gate electrode with low gate voltage (fully-gated IFET), we need additional considerations for the partial coverage of gate electrode (partially-gated IFET) as shown in Figure 2(a) with high gate voltage. The considerations are a fringing field effect and a counter-ion condensation as following.

Fringing field effect

Despite of difference in structure, the zeta potential modulation of partially-gated IFET could be similar to that of fully-gated IFET in physical intuition. Define 'gated region' as a region of gate electrode and 'non-gated region' as a region of absence of that. Gated and non-gated regions correspond to 'A' and 'B' denoted in Figure 2(a), respectively. Typically, when voltage is applied to the gate electrode, the electric field is sought to be generated only inside the oxide layer of gated region and the electric field abruptly drops to zero in that of non-gated region. However, this is impossible because of the conservative nature of the electric field, $\nabla \times \mathbf{E} = \mathbf{0}$[28]. To satisfy the conservation, the electric field should curve and extend

outward into non-gated region which is called fringing field effect or edge effect. Due to this fringing field, the zeta potential on oxide/electrolyte interface of non-gated region can be modulated as similar as gated region. The impact of fringing field was researched by Lin *et al*[29] using carbon nanotube FET (CNFET) where fringing field affected gating phenomena significantly. To solve fringing field directly, it requires high-cost computation. Numerical domain must be discretized into nearly zero sized elements in the vicinity of the each gate end, so that the number of degree of freedom diverges. To avoid this, we assumed that the distribution of the modulated zeta potential along the nanochannel wall followed the Gaussian distribution expressed as

$$f(x)=\frac{A}{\sigma\sqrt{2\pi}}\exp\left[-\frac{(x-\mu)^2}{2\sigma^2}\right] \tag{7}$$

where A is an arbitrary constant, σ is the standard deviation, and μ is the mean value of the arbitrary function $f(x)$, respectively. Using equation (7), the modulated zeta potential along the channel walls was set to be

$$\zeta(z)=\begin{cases}\zeta_{gate}\exp\left[-\dfrac{\left(z+\frac{L_{gate}}{2}\right)^2}{\alpha^2}\right] & \text{at} \quad z<-\dfrac{L_{gate}}{2} \text{ (region B)}\\ \zeta_{gate} & \text{at} \quad -\dfrac{L_{gate}}{2}\le z\le\dfrac{L_{gate}}{2} \text{ (region A)}\\ \zeta_{gate}\exp\left[-\dfrac{\left(z-\frac{L_{gate}}{2}\right)^2}{\alpha^2}\right] & \text{at} \quad z>\dfrac{L_{gate}}{2} \text{ (region B)}\end{cases}. \tag{8}$$

In above expressions, ζ_{gate} is the modulated zeta potential on oxide/electrolyte interface by gate electrode which is calculated from equations (1) ~ (6). α^2 is defined as $\alpha^2 = (L_{channel}-L_{gate})^2/4\ln\beta$ in which $L_{channel}$ is the length of the nanochannel, L_{gate} is the length of the gated region and $\beta=\zeta_{gate}/\zeta_{min}$ is ratio of modulated zeta potential and its minimum zeta potential at

the end of nanochannel wall. Since β is a phenomenological parameter, one can choose it in the range of 1 to ∞. For example of the limiting cases, β is equal to 1, corresponding to fully-gated system and β goes to infinity, diminishing the fringing field effect. We postulated that β was proportional to the electrical conductivity of the electrolyte solution and its values were summarized in SI Table 2.

Counter-ion condensation

Surface charge density, σ_s in SI Table 1 can be determined from the modulated zeta potential if charge-potential relation in electrokinetic system is known. In classical viewpoint, the Grahame equation based on the Poisson-Boltzmann equation can be used to determine the surface charge density. However, when zeta potential exceeds the thermal voltage, $RT/F \approx 25$mV, the electric double layer starts to enter a non-linear regime where the Grahame equation is expected to break down[23, 30, 31]. Under the conditions such as high zeta potential or high electrolyte concentration, one should consider the ion-ion interactions so that surface charge over-screening and ion crowding are arose in the vicinity of the solid/electrolyte interfaces. To elucidate those non-linear effects, additional compact layer consist of counter-ions has been proposed[30, 32]. In those literatures, counter-ions in the vicinity of the highly charged surface are condensed in narrow layer, and then new compact layer is formed beyond the Stern layer. Consequently, the impact of highly charged surface to the electric double layer structure is reduced by condensed counter-ions. To obtain charge-potential relation in that non-linear regime, Kilic and coworkers established the analytical model based on the modified Poisson-Boltzmann equation with a phenomenological parameter[30] which we chose in this work.

In their model, parameter ν represents the ratio of bulk electrolyte concentration (c_0) and maximum condensed concentration ($c_{\max}$) expressed by

$$\nu = \frac{2c_0}{c_{\max}} = 2a^3 N_A c_0 \tag{9}$$

where N_A is the Avogadro number and a is the effective diameter of an ion. Note that a is not necessarily the actual diameter of an ion is the order of 1 angstrom, it just means ion-ion correlation under phenomenological viewpoint. By definitions of (9), ν has a maximum value, 2 because c_0 cannot exceed the maximum concentration, $c_{\max}$. By their theoretical derivation without loss of generality, charge-potential relation became following form,

$$\sigma_s = 2\,\mathrm{sgn}(\zeta) ZFc_0\lambda_D \sqrt{\frac{2}{\nu}\ln\left[1 + 2\nu \sinh^2\left(\frac{ZF\zeta}{2RT}\right)\right]} \tag{10}$$

where λ_D is the Debye layer thickness defined as $\lambda_D = \sqrt{\left(\varepsilon_f RT\right)/\left(2Z^2F^2c_0\right)}$, sgn($\zeta$) is the sign of the zeta potential, and ζ is calculated from equation (8). The σ_s is used as the boundary conditions in SI Table 1. Due to highly confined nanostructure (radius in the order of 10 nm), ion-ion correlation were expected to be strong. To capture the strong correlation, the effective diameter of an ion, a, was fixed to be 7.5 nm[30], so that ν was proportional to the bulk electrolyte concentration from equation (9) of which values were summarized in SI Table 2.

Ionic current

To obtain theoretical *I-V* characteristics of IFET, local ionic current density, **i,** is defined by

$$\mathbf{i} = \sum_j Z_j F\left(-D_j\nabla c_j - \frac{Z_j F D_j}{RT} c_j \nabla\psi + c_j \mathbf{u}\right) \tag{11}$$

and then total ionic current through IFET system (I) can be calculated by

$$I = N_{ch}\int_S \mathbf{i}\cdot\mathbf{n}\mathrm{d}S \tag{12}$$

where N_{ch} is the number of nanochannel, S is arbitrary cross section of the system, and **n** is

normal vector on surface *S*. Required field quantities in equation (11) were obtained from equation (1) ~ (10) with governing equations and boundary conditions shown in supporting information.

RESULTS AND DISCUSSION

Ionic conductance at floating gate

Ionic transport in nanofluidic system has the unique property of surface-charge-governed regime demonstrated by D. Stein *et al*.[10] In a dilute limit, ionic conductance is independent from the bulk properties of the system such as the electrolyte concentration or the geometrical factor, so that the conductance curve saturates below a specific concentration value which is determined by surface charge density and called 'surface-charge-governed conductance'. Because the plateau of conductance curve is only revealed in nanochannel system, this property has been utilized to demonstrate the validity of the device in the view point of nanofluidic application. Beyond the specific concentration value, the conductance is proportional to the bulk concentration, called geometry-governed regime. These two distinct regimes can be plotted (ionic conductance as a function of bulk concentrations) simultaneously as shown in Figure 3. In a cylindrical nanochannel, the analytical expression of ionic conductance, G, was derived[33] as

$$G = \frac{\pi}{4}\frac{d_{nano}^2}{L_{nano}}\left[\left(\mu_{co}+\mu_{counter}\right)c_0F+\mu_{counter}\frac{4|\sigma_0|}{d_{pore}}\right] \quad (13)$$

where d_{nano} is the diameter of a nanochannel, L_{nano} is the length of a nanochannel, and μ_{co} and $\mu_{counter}$ is the electrophoretic mobility of co- and counter-ion, respectively. The first term in equation (14) represents the bulk conductance and the second term represents the surface-charge-governed conductance. Using equation (13) and circuit theory, the total conductance of our IFET at floating gate, G_{total}, was calculated from $G_{total}=80\times(G_{gated}\times G_{non\text{-}gated})/(2G_{gated}+G_{non\text{-}gated})$ in which G_{gated} and $G_{non\text{-}gated}$ are the ionic conductance of gated and non-gated region, respectively. We used values of $\mu_{co}=7.853\times10^{-8}$ $m^2/V\cdot s$, $\mu_{counter}=7.582\times10^{-8}$ $m^2/V\cdot s$, $|\sigma_0|=1.5$ mC/m^2, $d_{nano}=15$ nm (gated region) and 100 nm (non-gated region), and $L_{nano}=10$ um (gated region) and 5 um (non-gated region). Both theoretical (solid line) and

experimental (circles) conductance as a function of bulk concentration were shown in Figure 3. In a low concentration range (c_0<10^{-4} M), experiments were saturated to the surface-charge-governed conductance and consistent with analytical solution and the conductance fell into the geometry-governed regime above the concentration. However, in a high concentration range, *i.e.* c_0>10^{-1} M, the experiments were shown to be deviated from the theoretical calculation, while previous literatures followed the theoretical calculation over 1 M.[10, 33, 34]. The discrepancy would be come from highly confined microchannel. Our microchannels had the thickness of 1.5 um, while previous studies usually provided the demonstration with an open reservoir. The thin microchannel could provoke strong ion-ion interaction or ion-wall interaction in a high concentration range so that KCl solution at 10^{-1} M and 1 M concentration turned into a salt precipitation that hindered the ionic current through the micro-nanochannel since the precipitation acted as a physical obstacle. See the supporting information of the salt precipitation formation. In spite of the discrepancy in high concentration range, we concluded that our device was intact because surface-charge-governed conductance as the unique property of nanofluidic system was observed.

Ionic current with gate voltage

The ionic currents (I_D vs V_D) were measured as a function of gate voltage (V_G) at the concentration range from 10^{-5} M to 1 M as shown in Figure 4, demonstrating the Ohmic (or linear) relationship between I_D and V_D within the voltage range of $|V_D| < 2$ V. Over the range, one can have ion concentration polarization phenomena which involve a non-linear current-voltage relationship[35, 36]. Higher KCl concentration, we obtained higher ionic current values. Upon the application of gate voltage, ionic conductance increased regardless of the polarity of gate voltage for entire concentration range, called ambipolar behavior. A terminology of ‘ambipolar’ in MOSFET (Metal-Oxide-Semiconductor Field-Effect Transistor) represents

that the channel polarity strongly depends of the polarity of gate voltage. For instance, negative gate voltage induces abundant holes inside the channel, so that the channel becomes positive polarity and *vice versa*. In case of IFET, the same mechanism would be hold with near-zero surface charge. Thus, the increment of ionic current was proportional to the absolute value of the gate voltage. On the contrary, the ionic current should increase with either positive or negative gate voltage, if the IFET had unipolar characteristics. The ambipolar behavior was originated from that the nanochannel had extremely low surface charge density due to Al_2O_3 layer and the gate electrode had so-called an "all-around-gate structure" for the high sensitivity. The presenting devices had two distinguishable features; 1) sub-10nm channel size and 2) near-zero surface charge. The operation even at high electrolyte concentration would be beneficial from sub-10nm channel size since thinner geometry retains stronger perm-selectivity[6, 10]. The presenting high efficiency of gate modulation would be helped by the near-zero surface charge since the small change of gate voltage can be relatively large in the case of an extremely low surface charge[13, 14]. In order to show the robustness of the system, we simultaneously measured the leakage current from source to gate. SI Figure 3 showed that the leakage currents were below 4 pA and independent from the bulk concentrations, leading to a judgment that the leakage current would not effect on the ionic currents.

Electrokinetics of the ambipolar IFET

Because the IFET system involves a fluid with electricity, an analysis of electrokinetic fields such as electrostatic potential (ψ), averaged concentration distribution ($c_m \equiv (c_K + c_{Cl})/2$) and flow field (**u**) should be required for the characterization of the system. As we described in the numerical scheme section, those fields can be obtained by solving the coupled governing equations with the consideration of a fringing field effect and a counter-ion

condensation. Figure 5 ~ Figure 7 depicted electrostatic potentials, concentration fields, and flow fields inside the ambipolar IFET at the bulk concentration of 10^{-3} M and the applied drain voltage of 2 V. As shown in Figure 5, the electrostatic potential inside the nanochannel (-10 um < z < 10 um) varied according to the applied gate voltage. When the applied gate voltage was -2 V, large potential drop was occurred around z = 8 um because of the depletion of the charge carrier. In contrast, large potential drop was occurred near z = -8 um when V_G = +2 V. When V_G was 0.2964 V (≈ 0.3 V), the electrostatic potential was linearly dropped through the whole nanochannel because the nanochannel was modulated to zero polarity. These results were important since the application of gate voltage can drop the strength of the electric field (a slope of electrostatic potentials) around the gate electrode so that one can possibly lower the translocation velocity of charged molecules through the gated nanochannel. Especially, since the gated regions of nanochannels were transparent in our system, one can measure the speed *in situ*. Averaged concentration distributions were shown in Figure 6 in which each section (divided by breaks) denoted nanochannel regions in range of -8.1 um < z < -8 um, -5.07 um < z < -4.97 um, 4.97 um < z < 5.07 um, and 8 um < z < 8.1 um, respectively. As mentioned earlier, the depletion zone of the charge carrier was formed around z = 8 um at V_G = -2 V depicted as white region in Figure 6(a), and *vice versa* (Figure 6(c) of V_G = +2 V). Because the nanochannel became zero polarity at V_G = 0.2964 V, the electric double layer cannot be built up and concentration distributions should be uniform as shown in Figure 6(b). The flow fields depicted in Figure 7(a) and (c) demonstrated that vortical flows were generated adjacent the gated regions which were similar to the nanoporous membrane system[35-38]. As one can predict from the concentration distribution (Figure 6), a strong vortex (thick arrows) was formed at the depletion zone, while a weak vortical motion (thin arrows) was observed at the other side. This was because the lower concentration led to higher electric field (Figure 5) and strong electrokinetic flows. In Figure

7(b), any electrokinetic flows were not existed because of the absence of the electric double layer. Consequently, electrokinetic fields such as concentration distributions and flow fields can be inverted by the applied gate voltage.

Ambipolar characteristics (I_D-V_G as a function of V_D): Numerical matching

In an ambipolar IFET device, I_D-V_G characteristics become V-shaped curves since the ionic current should be modulated regardless of the polarity of gate voltage. On the contrary, an unipolar IFET has a diode behavior. The measured I_D-V_G characteristics were plotted in Figure 8 for different electrolyte concentrations with numerical results. The measured I_D-V_G characteristics were ambipolar (V-shaped curve) since an inherently low surface charge density of Al_2O_3 (-1.5 mC/m^2) and higher capacitance of an all-around-gate structure (~5 times) than that of a planar-gate effectively reflected the gate polarity.

In a low (10^{-5} M ~ 10^{-4} M) and an intermediate (10^{-3} M ~ 10^{-2} M) concentration range, numerical results were well-matched with experimental data. For 10^{-5} M and 10^{-4} M, the extent of the ionic current modulation was appeared in the same order of magnitude because those concentrations were in surface-charge-governed regime[10] where ion transport through the nanochannel is affected only by the surface charge density of nanochannel rather than bulk property. Meanwhile, deviations between measured and numerical results occurred in high concentration range (10^{-1} M ~ 1 M). Higher the bulk concentration gave larger deviation. Nevertheless, the measured I_D-V_G characteristics plotted in Figure 8 were ambipolar. Consequently, more constraints in theoretical considerations would be needed to describe the ion transport at extremely high concentration

The effects of fringing field and counter-ion condensation

We had adopted two additional constraints which were a fringing field effect and a counter-ion condensation to describe the ionic transportation through the partially gated IFET. Compared to the Poisson-Nernst-Planck-Stokes formulation without any constraints (dashed line in Figure 9), our modified formulation (solid line) was well-matched with experimental results. With a view point of the PNPS formulation without constraints, a positive gate voltage changed the polarity of gated region only, and then nanochannel behaved as the npn nanofluidic transistor for negatively charged nanochannel. For the npn nanofluidic transistor, the application of a drain voltage could cause a reverse bias in one of the two pn junctions and hence the ionic current should be saturated[39], leading to a unipolar behavior. Moreover, numerical results with negative gate voltage had non-negligible error compared to the experimental results. Therefore, the two constraints should be included in the PNPS formulation to correctly describe the ambipolar behavior of the presenting partially-gated IFET. The fringing fields which were generated in non-gated region to satisfy $\nabla \times \mathbf{E} = \mathbf{0}$ could modulate the whole nanochannel and hence the polarity of the entire nanochannel became positive or negative depending on the gate voltage, while the gate voltage was applied only near the center of nanochannel. Additionally, the condensed layer formed by counter-ion in the vicinity of the highly charged oxide/electrolyte interfaces let over-modulated surface charge drop down, so that the non-negligible numerical error at larger gate voltages was resolved. Therefore, fringing field effect and counter-ion condensation were essential constraints in IFET analysis.

Sensitive polarity inversion

The presenting IFET had lower threshold voltage to inverse the polarity of the nanochannel than previously reported IFETs[13, 16]. We defined the threshold voltage V_{th} as required gate voltage to regulate the zero-polarity of the nanochannel. When gate voltage was higher than

V_{th}, the nanochannel had the positive polarity and *vice versa*. Using the condition of $\sigma_0 = 0$ at $V_G = V_{th}$, we derived the simplified equation for V_{th} related to oxide capacitance C_{ox} and inherent surface charge density σ_0 as

$$V_{th} = -\frac{\sigma_0}{C_{ox}}. \quad (14)$$

Equation (14) presented that IFET with higher oxide capacitance and lower inherent surface charge density had lower threshold voltage, leading to a sensitive polarity inversion. Since Al_2O_3 used in this work had near-zero surface charge density (-1.5 mC/m^2) and capacitance of all-around-gate structure (5.06 mF/m^2) was 5 times higher than planar-gate structure, the threshold voltages of our device were calculated to be 0.2964 V from equation (14) and 0.2967 V from numerical simulations which were superior to other IFET's V_{th}[13, 16] as shown in Figure 10.

CONCLUSION

In this work, we developed a transparent all-around-gated ionic field effect transistor (IFET) which has an ambipolar characteristic and can be operated at wide range of electrolyte concentrations (10^{-5} M~1 M). Due to the relatively low oxide capacitance of a planar-gate structure and the inherently high surface charge density, a traditional IFET can only control the same polarity of charged species as the surface charge of nanochannel. To enable the polarity-independent control, all-around-gate structure was adapted to increase the efficiency of gate effect compared to the planar-gate structure and we used Al_2O_3 as oxide layer which has lower surface charge density than SiO_2. As a result, an ambipolar behavior was obtained by experiments and was validated by numerical simulations with a fringing field effect and a counter-ion condensation which had not been considered as major factors before. The numerical results demonstrated that the application of gate voltage can drop the strength of the electric field around the gated region so that one can possibly lower the translocation velocity of charged molecules through the nanochannel. In addition, the fabricated all-around-gated IFET had the lowest threshold voltage as required gate voltage to regulate the zero-polarity of the nanochannel. The use of this ambipolar IFET would provide significant advantages to cost-effective/on-demand/sensitive control of charged species such as ions (negative or positive), DNA (negative), RNA (negative), and proteins (negative or positive) regardless of their polarity which is important in a biomedical analysis such as biomolecule transport through nanochannels, medical diagnosis system, and point-of-care system, etc.

ACKNOLWLEDGMENTS

S.H. Lee, T. Jin and K.B. Kim were supported by the Pioneer Research Center Program (2012-0009563), Global Frontier Program (2014M3A6B2060301) through the National Research Foundation (NRF) of Korea funded by the Ministry of Science, ICT & Future Planning and Seoul National University Brain Fusion Program Research Grant.

H. Lee, S. Park and S. J. Kim were supported by Basic Science Research Program (2013R1A1A1008125), the Center for Integrated Smart Sensor funded as Global Frontier Project (CISS- 2011-0031870) and Future based Technology Development Program (Nano Fields) (2012-0001033) by the Ministry of Science, ICT & Future Planning and Korean Health Technology RND project, Ministry of Health and Welfare Republic of Korea (HI13C1468, HI14C0559)

FIGURE CAPTIONS

Figure 1. (a) Schematics of fabrication process. (b) The schematic diagram of all-around-gated IFET. Cross-sectional SEM images of (c) non-gated region and (d) gated region. (e) Microscopic image of IFET device near nanochannel array.

Figure 2. (a) Schematic representation of numerical domain (not to scale). A and B denoted the gated and non-gated region. (b) The actual numerical domain.

Figure 3. Ionic conductance as a function of bulk concentration. Experimental conductance and analytical solutions were denoted by open circles and solid line, respectively. The plot clearly demonstrated a nanofluidic characteristic of surface-charge- and geometry-governed regime.

Figure 4. Experimentally measured I_D-V_D characteristics in the concentration range of 10^{-5} M to 1 M. The conductance increased as a function of the absolute value (regardless of the polarity) of V_G.

Figure 5. Electrostatic potential as a function of z-axis at V_D = +2 V. The gated region laid between z = -5 um and z = 5 um.

Figure 6. Spatial distributions of averaged concentrations ($c_m = (c_K+c_{Cl})/2$). On these figures, the left side was source (electrostatically ground) and the right side was drain (2 V). Bulk concentration was fixed to 10^{-3} M. The applied gate voltage (V_G) was varied in each figure. Breaks denoted nanochannel regions in range of -8.1 um < z < -8 um, -5.07 um < z < -4.97 um, 4.97 um < z < 5.07 um, and 8 um < z < 8.1 um, respectively.

Figure 7. Spatial distributions of electrokinetic flow fields. Voltage configurations and bulk concentration were the same as Figure 6. Solid lines were the stream lines and arrows were flow directions and strengths.

Figure 8. Experimental and numerical I_D-V_G at each electrolyte concentration. The "V" shape represented the ambipolar behavior.

Figure 9. Numerical matching of PNP theory and our new model with experimental values that were measured at V_D = +2 V. Bulk electrolyte concentration, c_0 was (a) 10^{-5} M and (b) 10^{-3} M.

Figure 10. Threshold voltages of various IFET devices. Planar-gate on thick SiO_2 (□) and planar-gate on thin SiO_2 (Δ) were referred from literatures[13, 16].

REFERENCES

1. H. Daiguji, P. Yang, A. J. Szeri and A. Majumdar, *Nano Letters*, 2004, **4**, 2315-2321.
2. W. Guo, L. Cao, J. Xia, F.-Q. Nie, W. Ma, J. Xue, Y. Song, D. Zhu, Y. Wang and L. Jiang, *Advanced Functional Materials*, 2010, **20**, 1339-1344.
3. M. Wanunu, W. Morrison, Y. Rabin, A. Y. Grosberg and A. Meller, *Nat Nano*, 2010, **5**, 160-165.
4. Y. Kim, K. S. Kim, K. L. Kounovsky, R. Chang, G. Y. Jung, J. J. dePablo, K. Jo and D. C. Schwartz, *Lab Chip*, 2011, **11**, 1721-1729.
5. T. C. Kinnaman, *Ecological Economics*, 2011, **70**, 1243-1249.
6. S. J. Kim, S. H. Ko, K. H. Kang and J. Han, *Nat Nano*, 2013, **8**, 609-609.
7. D. Fologea, J. Uplinger, B. Thomas, D. S. McNabb and J. Li, *Nano Lett.*, 2005, **5**, 1734-1737.
8. M. Utkur, C. Jeffrey, D. Valentin, A. Aleksei and T. Gregory, *Nanotechnology*, 2010, **21**, 395501.
9. M. Wanunu and A. Meller, *Nano Lett.*, 2007, **7**, 1580-1585.
10. D. Stein, M. Kruithof and C. Dekker, *Physical Review Letters*, 2004, **93**, 035901.
11. R. Karnik, K. Castelino, R. Fan, P. Yang and A. Majumdar, *Nano Letters*, 2005, **5**, 1638-1642.
12. R. Karnik, R. Fan, M. Yue, D. Li, P. Yang and A. Majumdar, *Nano Lett.*, 2005, **5**, 943-948.
13. R. Fan, M. Yue, R. Karnik, A. Majumdar and P. Yang, *Phys. Rev. Lett.*, 2005, **95**, 086607.
14. R. Fan, S. Huh, R. Yan, J. Arnold and P. Yang, *Nat Mater*, 2008, **7**, 303-307.
15. U. Vermesh, J. W. Choi, O. Vermesh, R. Fan, J. Nagarah and J. R. Heath, *Nano Lett.*, 2009, **9**, 1315-1319.
16. W. Guan, R. Fan and M. A. Reed, *Nat Commun*, 2011, **2**, 506.
17. B. Kim, J. Heo, H. J. Kwon, S. J. Cho, J. Han, S. J. Kim and G. Lim, *ACS Nano*, 2013, **7**, 740-747.
18. J. Heo, H. J. Kwon, H. Jeon, B. Kim, S. J. Kim and G. Lim, *Nanoscale*, 2014, **6**, 9681-9688.
19. S. H. Tan, N. T. Nguyen, Y. C. Chua and T. G. Kang, *Biomicrofluidics*, 2010, **4**, 32204.
20. S.-W. Nam, M. J. Rooks, K.-B. Kim and S. M. Rossnagel, *Nano Lett.*, 2009, **9**, 2044-2048.
21. S.-W. Nam, M.-H. Lee, S.-H. Lee, D.-J. Lee, S. M. Rossnagel and K.-B. Kim, *Nano Lett.*, 2010, **10**, 3324-3329.
22. G. Pardon and W. van der Wijngaart, *Adv. Colloid Interface Sci.*, 2013, **199–200**, 78-94.
23. Z. Jiang and D. Stein, *Langmuir*, 2010, **26**, 8161-8173.
24. Z. Jiang and D. Stein, *Phys. Rev. E*, 2011, **83**, 031203.
25. L.-H. Yeh, S. Xue, S. W. Joo, S. Qian and J.-P. Hsu, *The Journal of Physical Chemistry C*, 2012, **116**, 4209-4216.
26. C. Hughes, L.-H. Yeh and S. Qian, *The Journal of Physical Chemistry C*, 2013, **117**, 9322-9331.

27. N. Hu, Y. Ai and S. Qian, *Sensors and Actuators B: Chemical*, 2012, **161**, 1150-1167.

28. R. K. Wangsness, *Electromagnetic fields*, Wiley, 1986.

29. Y.-M. Lin, J. Appenzeller and P. Avouris, *Nano Lett.*, 2004, **4**, 947-950.

30. M. S. Kilic, M. Z. Bazant and A. Ajdari, *Phys. Rev. E*, 2007, **75**, 021502.

31. W. B. Russel, D. A. Saville and W. R. Schowalter, *Colloidal Dispersions*, Cambridge University Press, 1992.

32. G. S. Manning, *The Journal of Physical Chemistry B*, 2007, **111**, 8554-8559.

33. R. M. M. Smeets, U. F. Keyser, D. Krapf, M.-Y. Wu, N. H. Dekker and C. Dekker, *Nano Lett.*, 2005, **6**, 89-95.

34. B. S. Reto, H. Jongyoon and R. Philippe, *Rev. Mod. Phys.*, 2008, **80**, 839.

35. I. Cho, G. Sung and S. J. Kim, *Nanoscale*, 2014, **6**, 4620-4626.

36. S. J. Kim, Y.-C. Wang, J. H. Lee, H. Jang and J. Han, *Phys. Rev. Lett.*, 2007, **99**, 044501.

37. E. V. Dydek, B. Zaltzman, I. Rubinstein, D. S. Deng, A. Mani and M. Z. Bazant, *Physical Review Letters*, 2011, **107**, 118301.

38. S. J. Kim, S. H. Ko, R. Kwak, J. D. Posner, K. H. Kang and J. Han, *Nanoscale*, 2012, **4**, 7406-7410.

39. L.-J. Cheng and L. J. Guo, *ACS Nano*, 2009, **3**, 575-584.

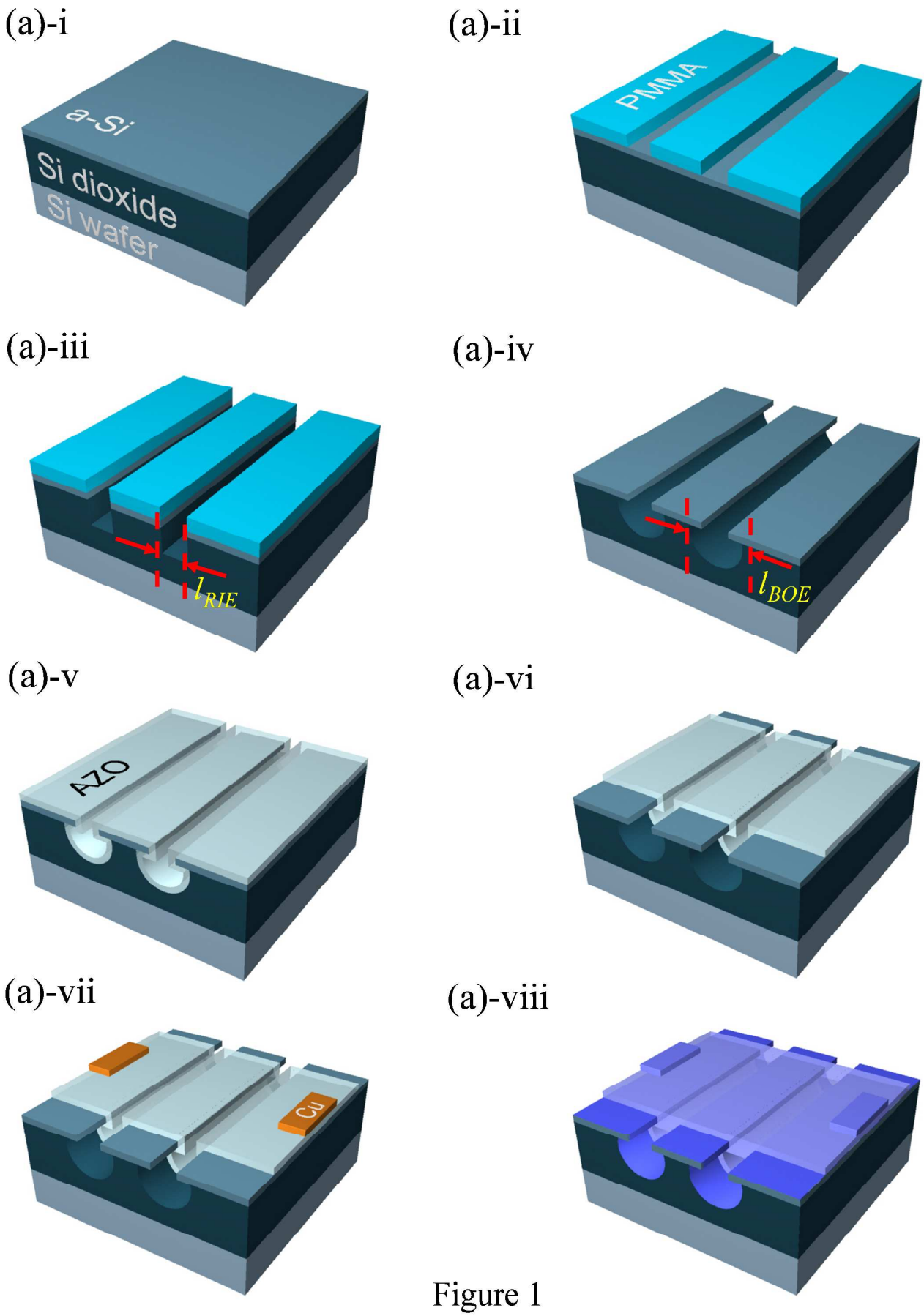

Figure 1

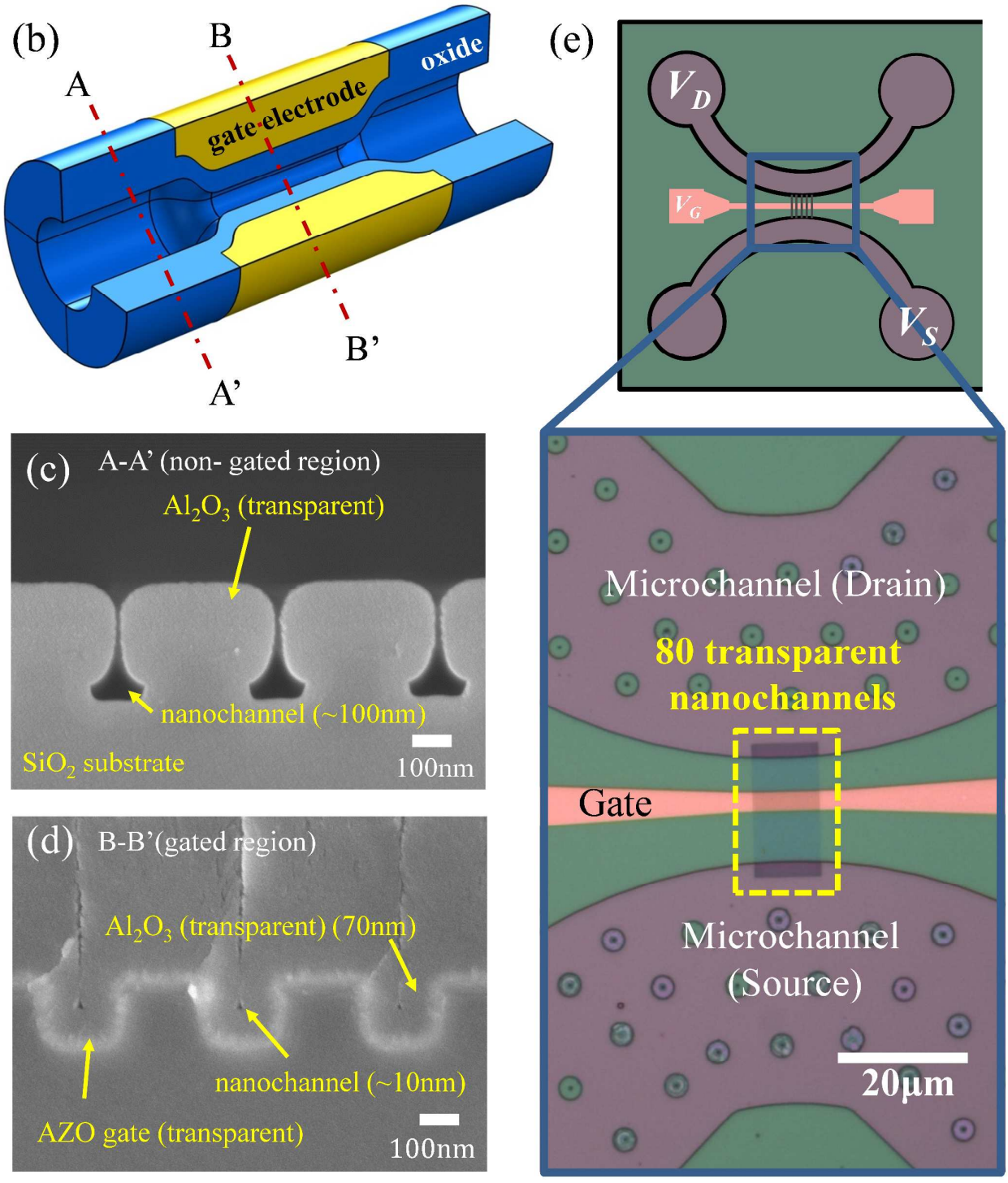

Figure 1

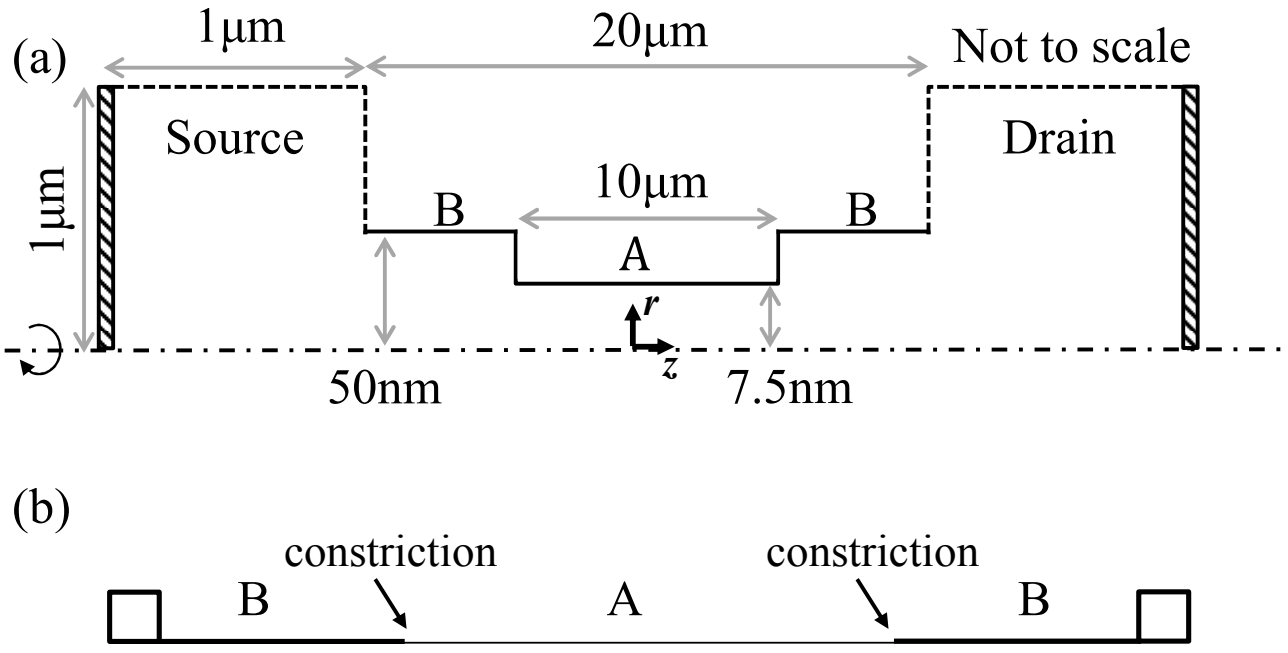

Figure 2

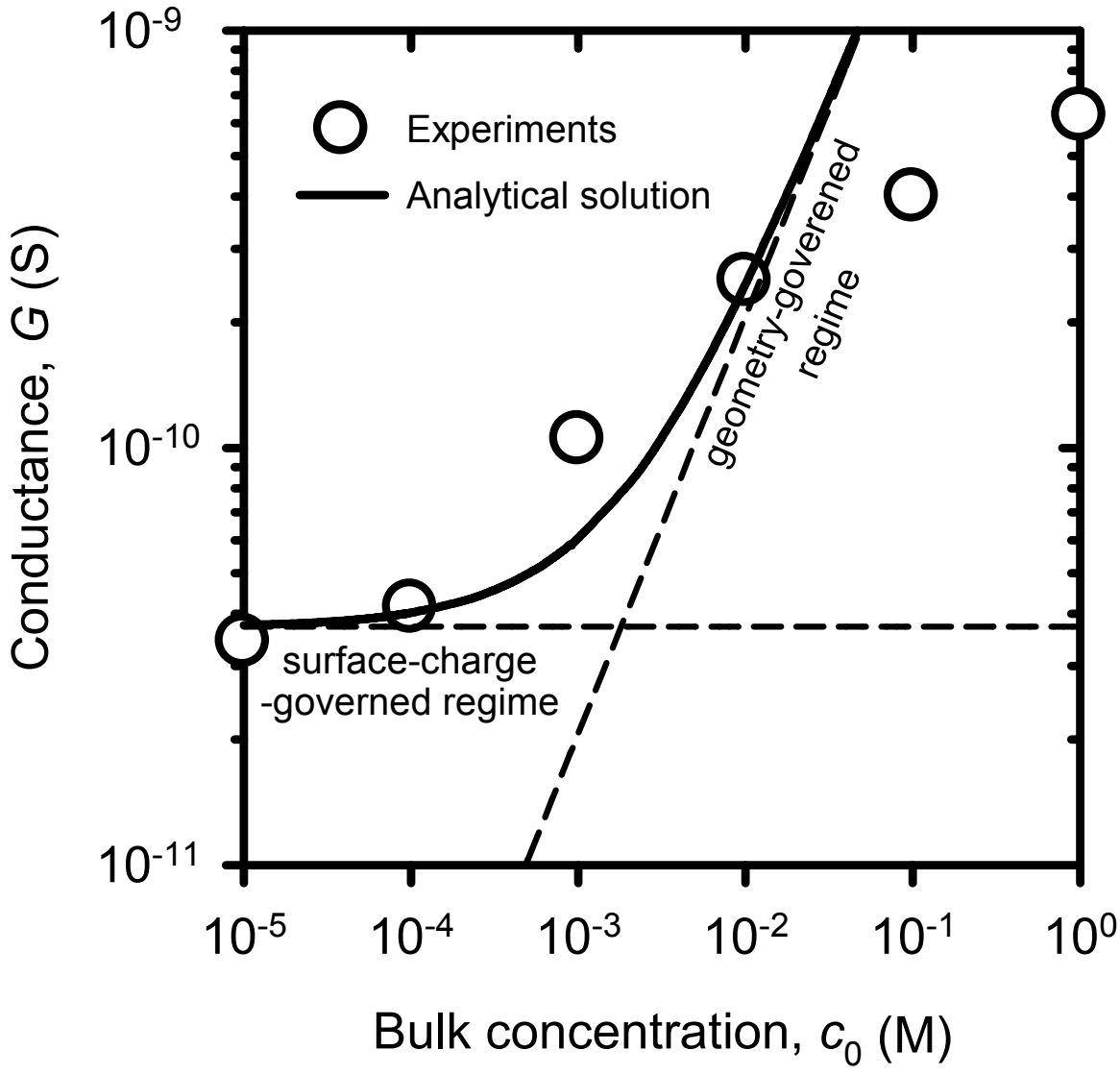

Figure 3

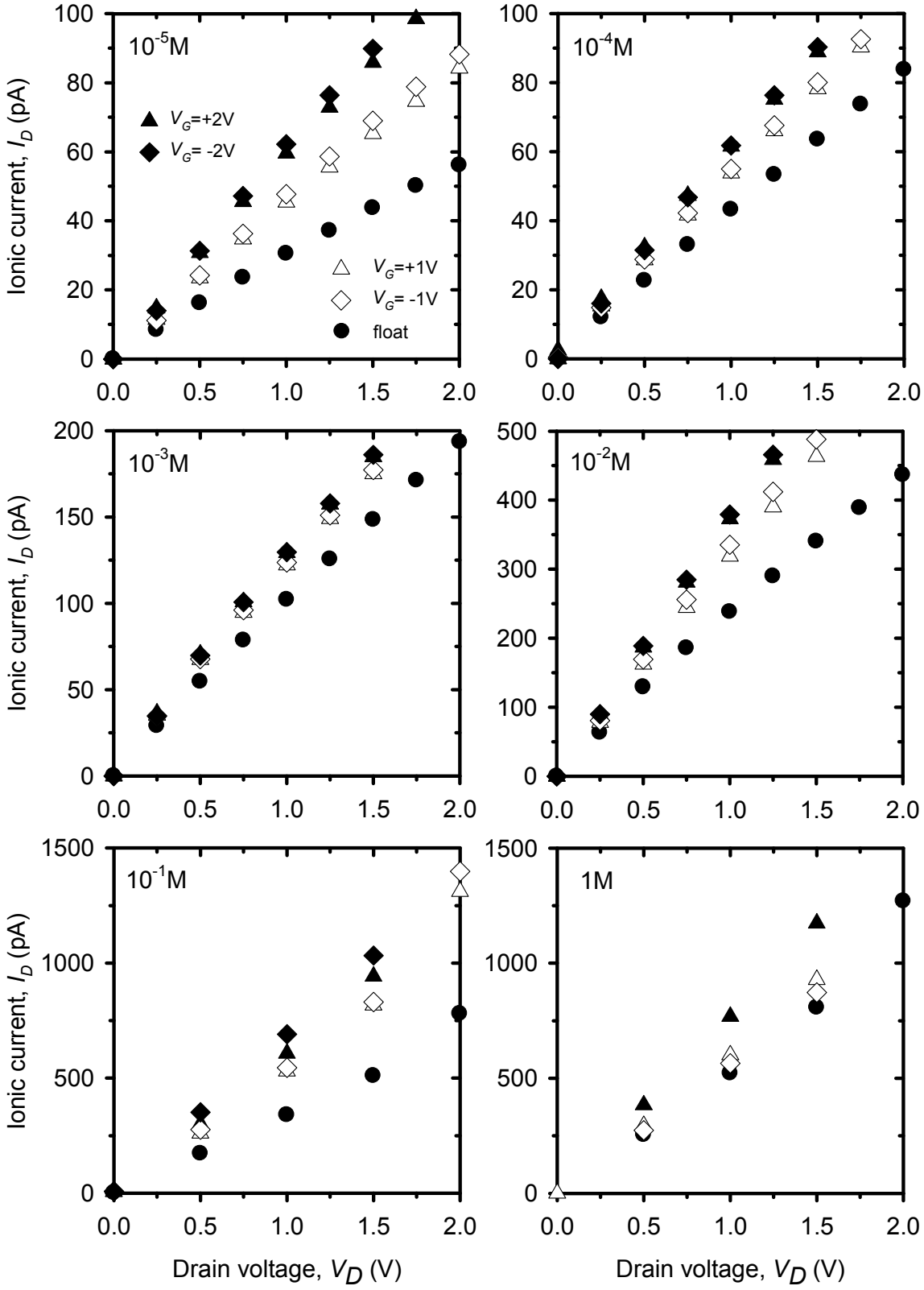

Figure 4

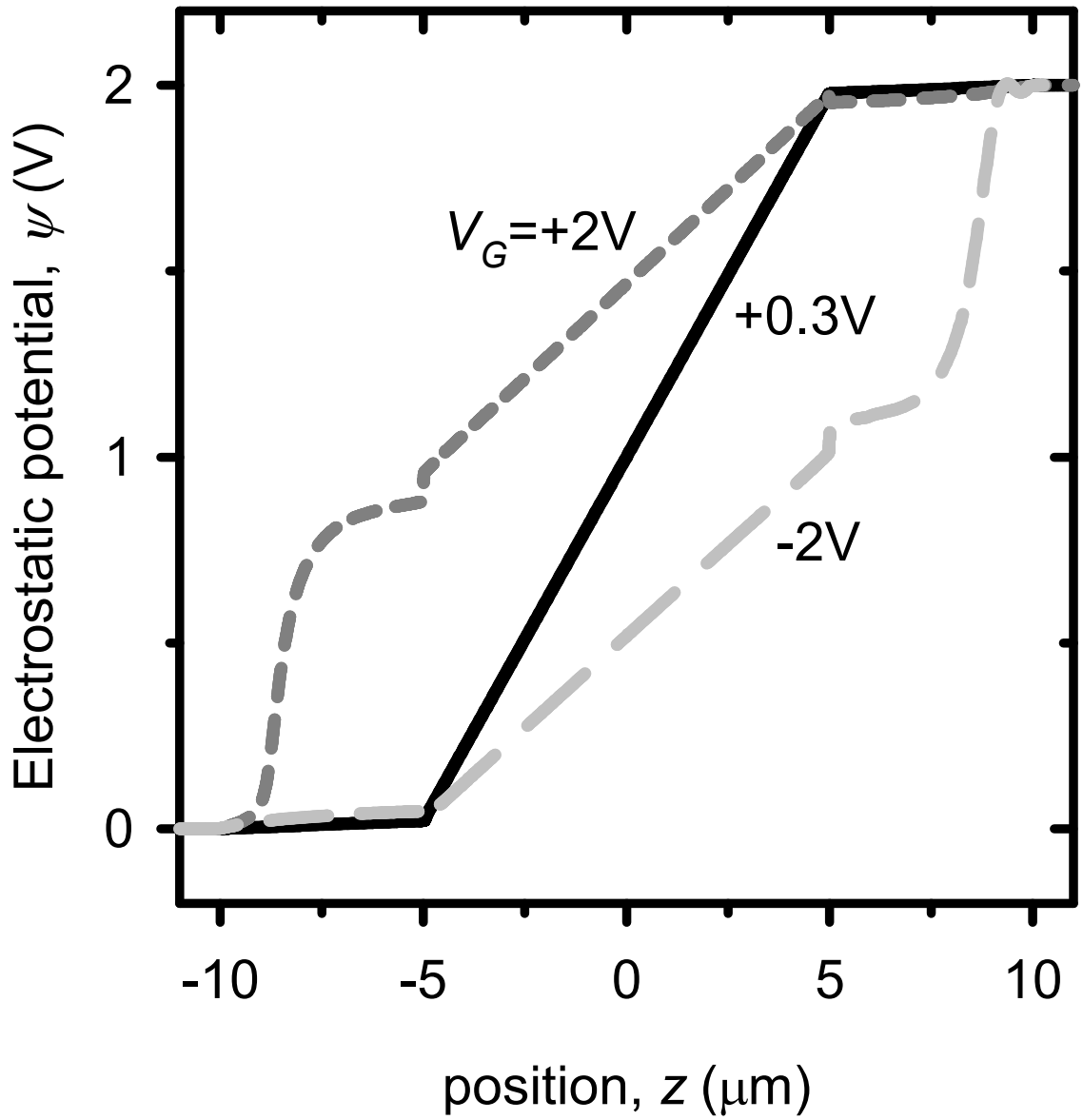

Figure 5

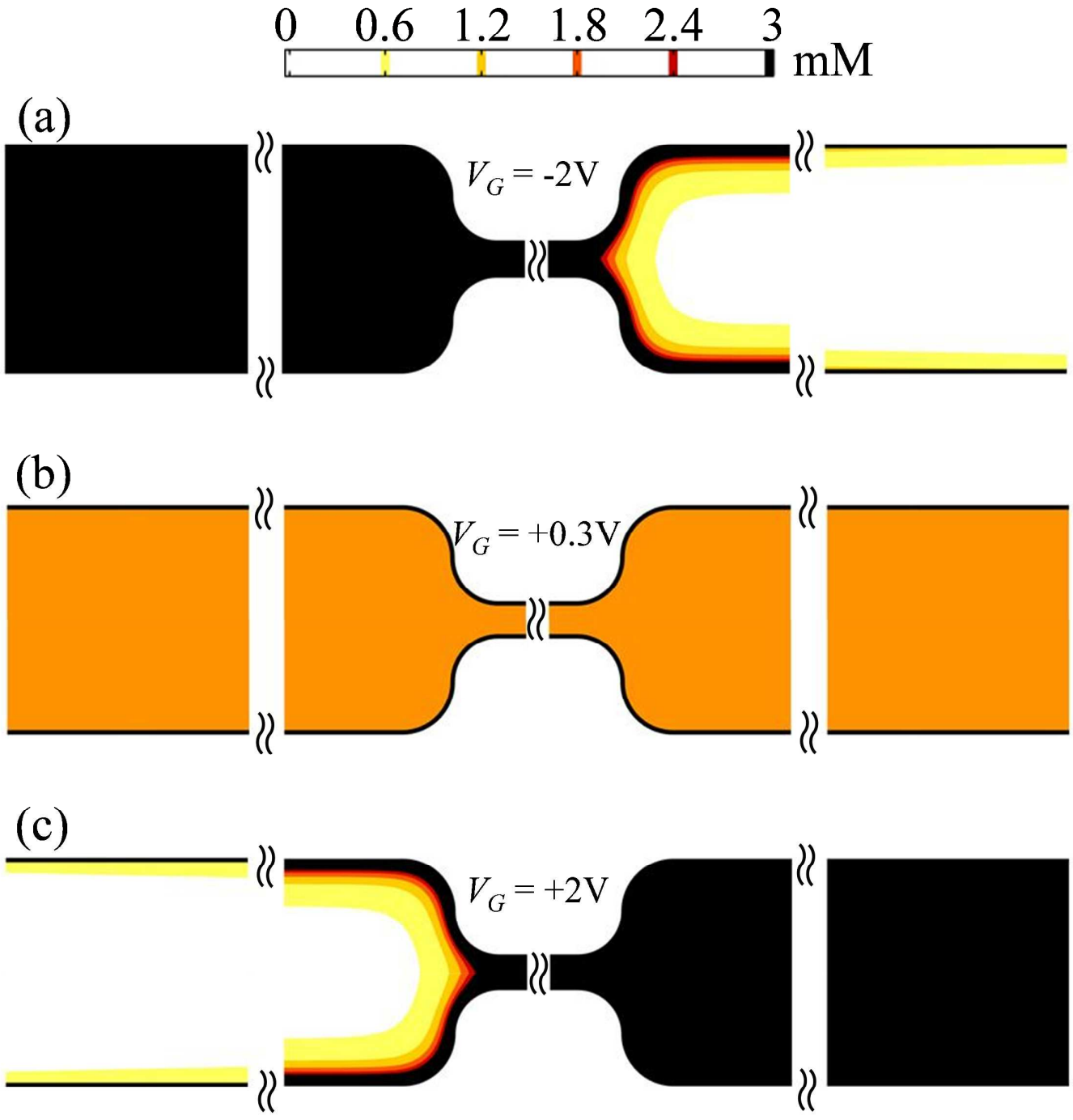

Figure 6

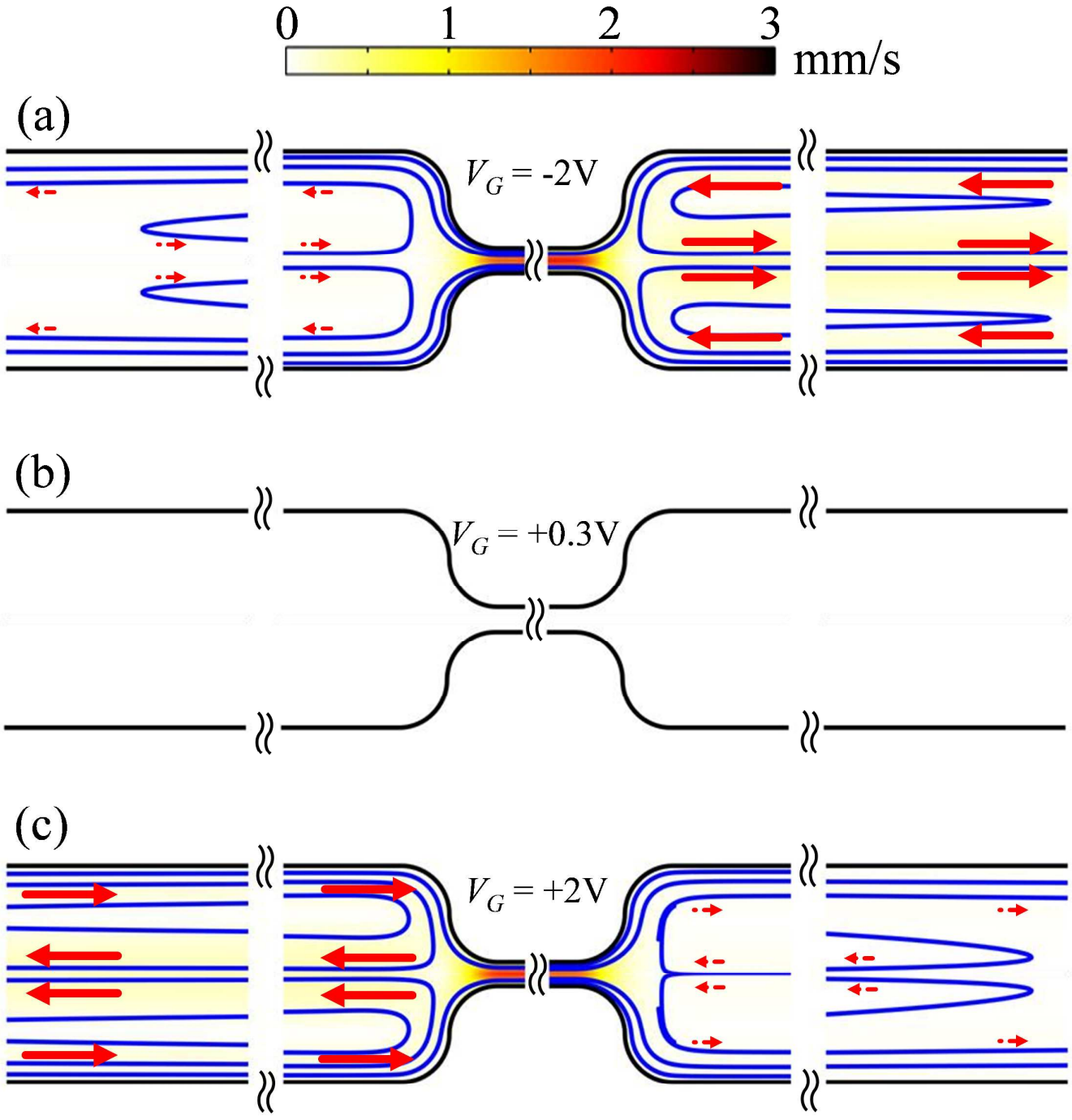

Figure 7

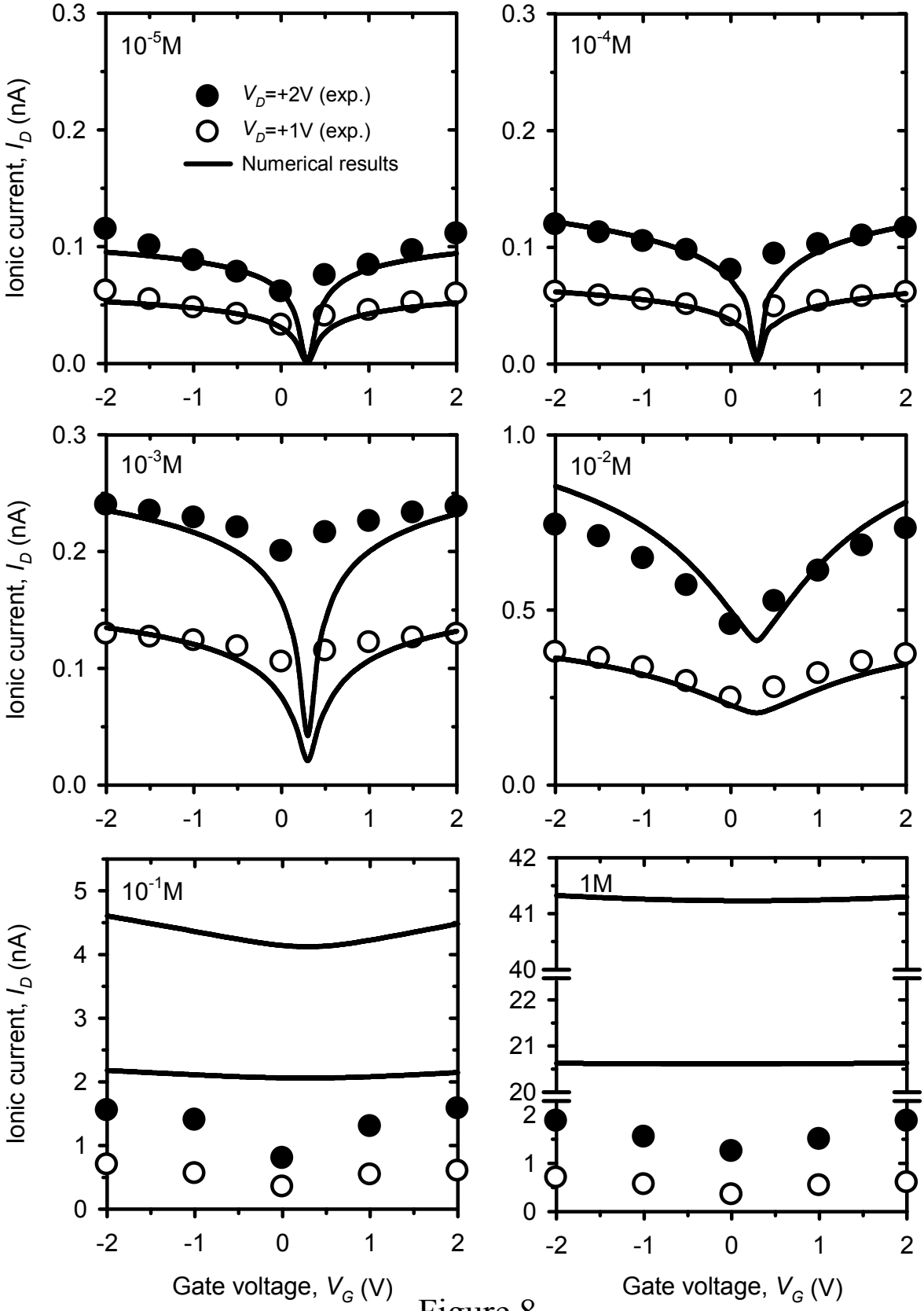

Figure 8

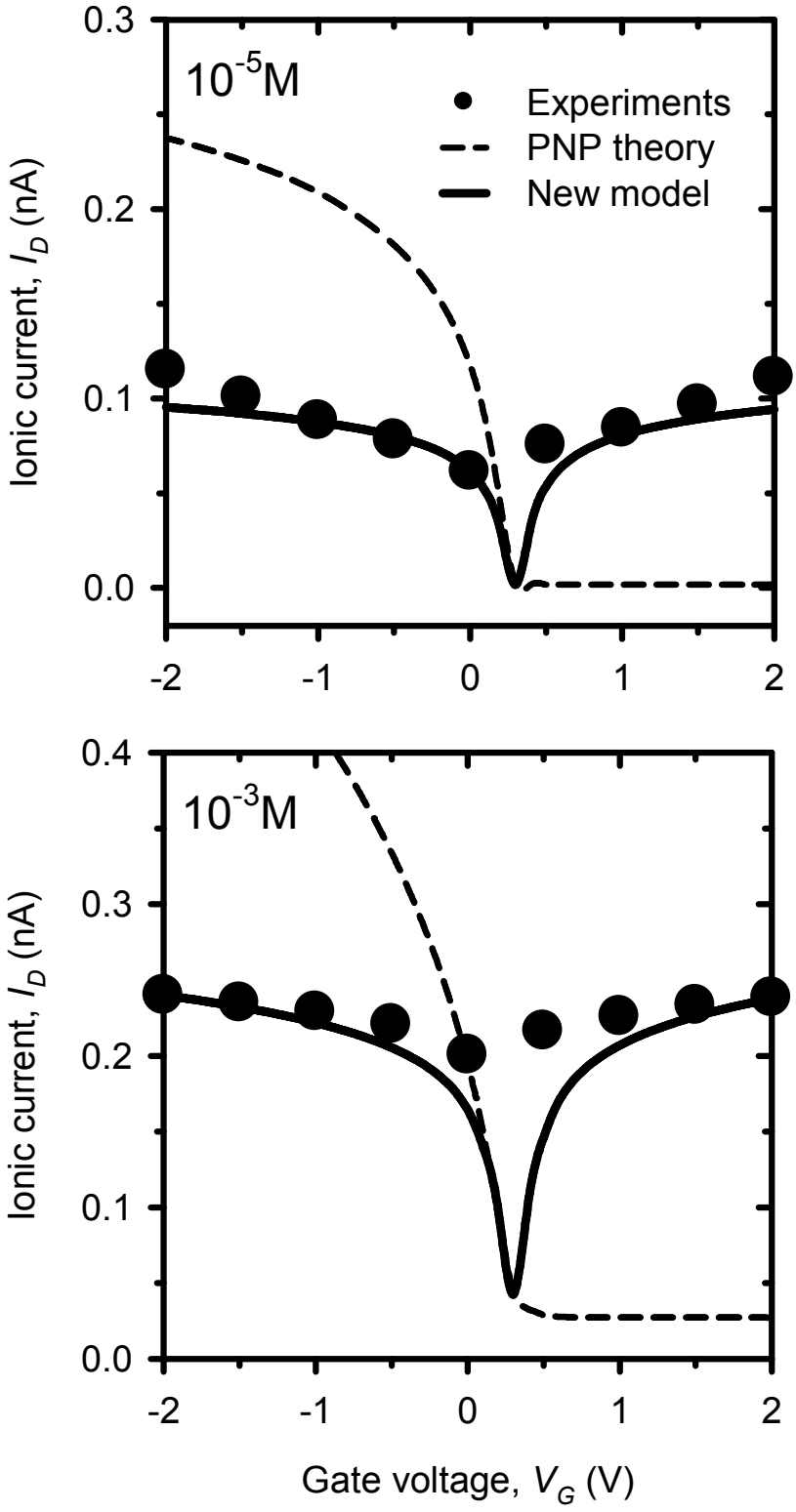

Figure 9

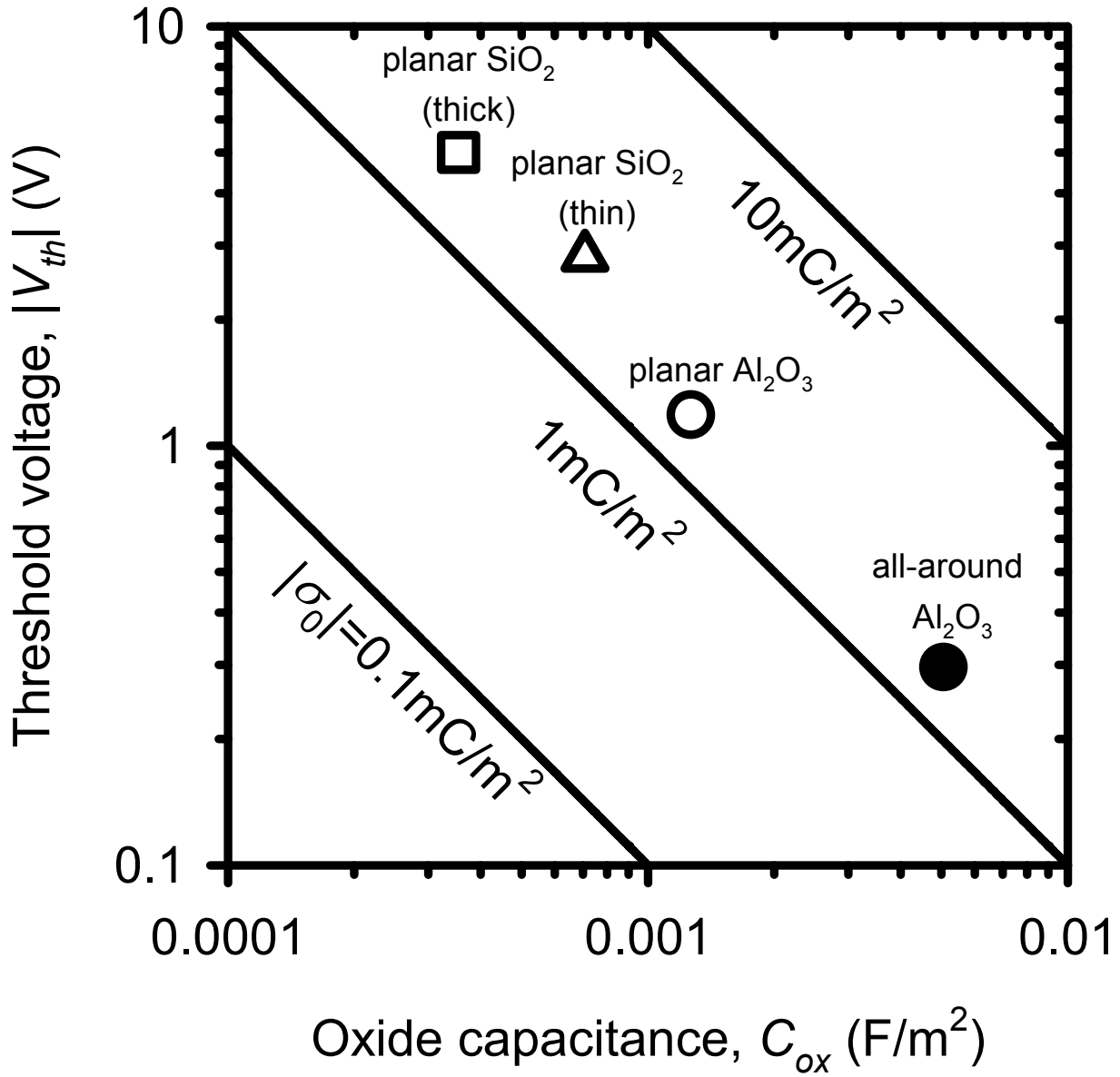

Figure 10